A motion tracking approach to position marine floating structures based on measured acceleration and angular velocity

Fushun Liu[a,*], Shujian Gao[a], Yong Liu[a], Dianzi Liu[b]

[a]*Shandong Province Key Laboratory of Ocean Engineering, Ocean University of China, Qingdao 266100, China*
[b]*Engineering, Faculty of Science, University of East Anglia, Norwich, NR4 7TJ, UK*

Abstract

One of the major challenges arising from dynamic response measurement of floating structures is to effectively track their 6DOF response in harsh environments. Although the combination of GPS and INS techniques has the ability to estimate the positioning of floating structures, it is tedious that the corrections of response measurements have to be carried out at regular intervals due to the low accuracy, instability and various harsh environments. Aiming at achieving long-term stable and efficient measurements of floating structural responses, an indirect contact motion tracking approach based on the combination of the accelerations and angular velocities has been proposed in this paper. First, a novel displacement reconstruction model has been established to effectively determine the translational displacements of floating structures. Following that, to correct the errors of tilt and coordinate data from the measured accelerometers, the quaternion method has been applied to update the dynamic Euler angle. The major contributions of this research include: 1) the development of a non-integral drift-free method for displacement reconstructions without GPS and 2) the realization of a synchronous tracking system considering dynamic tilt error of accelerometers for floating structures with the motions in 6-DOF. To demonstrate the correctness of the proposed approach, two numerical examples have been examined to track the motion of floating structures. Numerical results have shown that the maximum error of the reconstructed displacement between the proposed approach and Orcaflex is only 0.8096%, indicating their good agreement. Then, a physical experiment of a semi-submersible platform under the action of regular and irregular waves has been conducted to verify the feasibility of the developed tracking approach by comparison of the data from the traditional optical device and camera. The results show that the proposed method has the ability to effectively predict the operation conditions of floating structures and provides a valuable insight into the development of an efficient synchronous tracking system for various engineering applications.

Keywords: Floating structure; 6-DOF motion; acceleration; angular velocity; response tracking

1. Introduction

With the continuous depletion of land resources and the increasing energy demand of human activities, the development and utilization of marine resources have become an important way to moderate this contradiction between supply and demand (Wu and Gao, 2021; Zhang et al., 2021). Due to the gradual increase of the developed water depth, the requirement of marine engineering equipment was envisaged for the expansion of offshore survey into deep sea exploration, and then various deep-sea floating structures came into being (Fu and Moan, 2012; Wei et al., 2018). Besides facing more complex and diverse external excitations, floating structures in the service process will also bear the action of new types of excitations such as internal waves (Ai et al., 2021) and abnormal waves (Veltcheva and Soares, 2016), which will lead to the large deformation and strong nonlinearity. Therefore, to ensure the safety of personnel and working condition of structures, accurate testing and tracking of the operation state of structures have become the primary consideration (Liu et al., 2020). However, the service environment of floating structures is usually far from land, and the conventional methods at the laboratory-scale can not meet the measurement requirements of floating structures. For example, the optical three-dimensional tracking system needed a fixed reference point in the test process, and could not be directly applied to the motion measurement of floating structures (Kim et al., 2020).

Taking into account the special working environment of floating structures and the difficulty of using a single measurement technology to predict structural responses, it is necessary to apply a variety of different measurement technologies to jointly track the motions of the structure (Wu et al., 2016). At present, the motion tracking of floating structures is mainly based on the angular velocity measured by gyroscope and the linear displacement measured by GPS. The Oryx company (Prislin et al., 1999) installed the world's first Spar platform in the Gulf of Mexico, and tested the 6-DOF motion responses of the structure using two GPS equipment and inclinometer, respectively. The BMT company (Edwards et al., 2005) developed the earliest deepwater floating platform monitoring system - called CONOCO Joliet TLWP, to monitor the hydrometeorology, current profile, platform position and 6-DOF structural motions, which were realized by GPS and gyroscope, respectively. Du et al. (2013) also developed a motion monitoring system, which was installed and tested on the LH11-1 semisubmersible platform in South China sea. As the motion tracking of floating structures based on gyroscope and GPS has been widely investigated, theories including geometric framework (Mitikiri and Mohseni, 2021), Kalman filter (Chen et al., 2019) and quaternion method (Chen et

*Corresponding author: percyliu@ouc.edu.cn (Fushun Liu).

al., 2021) for the calculation of structural dynamic Euler angles based on the angular velocity measured by gyroscope have been widely used and lead to high-precision results for the dynamic Euler angle. However, the measured values encountering the issue of data error or even complete loss, mainly include data jump, drift and instability, which will cause the system to dislocate the structure, or drive the structure to the wrong target position, and then result in accidents (Nezhadshahbodaghi and Mosavi, 2021).

Chen et al. (2009) summarized five DGPS failures of drilling platforms in Norway, and results showed that the data mutation caused by DGPS failure might involve tens of meters of the position change, and the maximum data jump reached 65m. In addition, there were many sudden changes of positions from 10m to 20m in the process of dynamic positioning. Similarly, in the performance monitoring of marlin TLP from 2003 to 2005, it could be seen that even under normal conditions, the sudden drift of more than 10m was identified in the structural motion response (Liagre et al., 2008). The phenomenon of data drift was more serious under the action of worse marine environments, such as hurricane. Teigen and Haver (1998) compared the numerical response of Heidrun TLP structure of 10 motion responses including wave heights between 4m and 10m with the measured results, and found that the deviation between the measurement error and the model prediction was as high as 20%. To overcome the problems of the low accuracy, instability and environment dependence of GPS, some scholars used the contact sensors (accelerometer and gyroscope) to test the dynamic acceleration and angular velocity of the structure, and then the 6-DOF motion could be tracked through the measured data. However, in the process of using acceleration to solve the dynamic displacement of the structure, a new problem has arisen (Damaris and Jaime, 2018), that is, the displacement calculated by the direct integration has a serious drift due to the influence of unknown initial conditions, the sensor baseline drift and environmental noise.

To reconstruct the displacement from the measured accelerations, many scholars have carried out relevant research. Hong et al. (2010) applied the variational approach to the minimum problem to derive the reconstructed governing equation for the determination of displacements. Thus, the displacement and velocity of the structure were reconstructed by FIR filter using the finite element method. Based on Chebyshev polynomials, Gao et al. (2021) used the high pass filter to remove the drift components, and realized the displacement reconstruction of offshore wind turbines using the measured accelerations. Zheng et al. (2019) developed an online and real-time displacement reconstruction method using a baseline correction technology. Employing recursive least squares, a recursive high-pass filter and a recursive integration, the structural displacement was reconstructed. However, the aforementioned methods are categorized as a class

of the filtering methods, in which the accuracy of results is poor as the drift term can not be removed duration the displacement reconstruction process for floating structures dominated by low-frequency. To avoid the drift problem caused by integration, Liu et al. (2021) developed a non-integral displacement reconstruction method based on the complex exponential representation of accelerations and realized the high-precision reconstruction of dynamic displacements.

To improve the long-term stable and high-precision measurements of floating structures, a novel motion tracking method based on the measured acceleration and angular velocity has been developed in this paper. Three contributions have been achieved as follows: 1) to correct the measured acceleration using the calculated Euler angle by the quaternion method under the condition of the field test environment and sensor tilt; 2) to reconstruct the displacement by modifying the accelerations in a non-integral drift-free way; 3) to realize a 6-DOF high-precision motion tracking as well as avoid the serous environmental interference and data loss of the GPS. The rest of this paper is structured in the following Sections. The quaternion and coordinate transformation methods used in this paper have been introduced in Section 2. Then, the proposed 6-DOF motion tracking method for floating structures has been described in Section 3. Its correctness has been verified by two numerical examples including a single-DOF system and a semi-submersible platform in Section 4 and 5. Finally, the physical model of the semi-submersible platform under the action of regular and irregular waves in Section 6 has been examined to demonstrate the potential application and feasibility of the proposed method.

2. Preliminaries

2.1. Coordinate transformation

Due to the complex measurement environment and safety considerations, the location of the sensor installation may not be the most suitable place, which may affect the measurement results. Therefore, in order to obtain the dynamic response at the center of gravity (COG), it is necessary to perform the coordinate transformation. To realize the transformation of motion response at different positions, two sets of coordinate systems are needed: one is fixed at the center of the structure, expressed as the $oxyz$, and the other is fixed at the test point denoted as the $\hat{o}\hat{o}\hat{y}\hat{z}$ in Fig. 1.

Let α, β and θ represent the Euler angles of rotation of the structure about the x, y and z axes, respectively (as shown in Fig. 1). The relationship between the coordinate systems $\widehat{o\widehat{x}\widehat{y}\widehat{z}}$ and $oxyz$ can be obtained

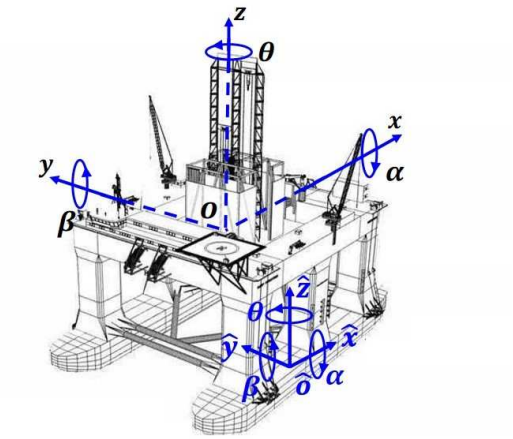

Fig. 1: The diagrams of six degrees of freedom movement and coordinate transformation of floating structures.

by the coordinate transformation (Makdah et al., 2019) as:

$$\begin{bmatrix} z \\ y \\ z \end{bmatrix} = \begin{bmatrix} 1 & 0 & 0 \\ 0 & cos\alpha & -sin\alpha \\ 0 & sin\alpha & cos\alpha \end{bmatrix} \begin{bmatrix} cos\beta & 0 & sin\beta \\ 0 & 1 & 0 \\ -sin\beta & 0 & cos\beta \end{bmatrix} \begin{bmatrix} cos\theta & -sin\theta & 0 \\ sin\theta & cos\theta & 0 \\ 0 & 0 & 1 \end{bmatrix} \begin{bmatrix} \widehat{x} \\ \widehat{y} \\ \widehat{z} \end{bmatrix} = [L][M][N] \begin{bmatrix} \widehat{x} \\ \widehat{y} \\ \widehat{z} \end{bmatrix} \quad (1)$$

where $[L]$, $[M]$ and $[N]$ represent the rotation matrix of the coordinate system $\widehat{ox}\widehat{y}\widehat{z}$ about the $\widehat{ox}$, $\widehat{oy}$ and $\widehat{oz}$ axes, respectively.

Let $\mathbf{T} = [L][M][N]$, one can obtain

$$\mathbf{T} = \begin{bmatrix} cos\beta cos\theta & -cos\beta sin\theta & sin\theta \\ sin\alpha sin\beta cos\theta + cos\alpha sin\theta & -sin\alpha sin\beta sin\theta + cos\alpha cos\theta & -sin\alpha cos\beta \\ -cos\alpha sin\beta cos\theta + sin\alpha sin\theta & cos\alpha sin\beta sin\theta + sin\alpha cos\theta & cos\alpha cos\beta \end{bmatrix} \quad (2)$$

where $\mathbf{T}$ represents the transformation matrix of two coordinate system.

2.2. Quaternion definition

Quaternion method, invented by Hamiltion, is a generalization of complex numbers in the four-dimensional real number space $\mathbb{R}^4$, which can be defined as $q = [s, \mathbf{v}]$, where s and $\mathbf{v}$ represent the scalar and vector parts, respectively. Quaternion satisfies (Grigoryan and Agaian, 2022; Urynbassarova et al., 2022):

$$\begin{cases} q_1 + q_2 = [s_1 + s_2, \mathbf{v}_1 + \mathbf{v}_2] \\ \lambda q = [\lambda s, \lambda \mathbf{v}] \end{cases} \quad (3)$$

where λ represents a scalar. And the multiplication rule for quaternion is defined as:

$$q_1 \bigotimes q_2 = [s_1 s_2 - \mathbf{v}_1 \cdot \mathbf{v}_2, s_1 \mathbf{v}_2 + s_2 \mathbf{v}_1 + \mathbf{v}_1 \times \mathbf{v}_2] \tag{4}$$

According to Euler theorem, the motion of a rigid body at any fixed point can be equivalent to the rotation about the axis passing through the fixed point. Thus, the rotation in a coordinate system with the magnitude φ about the unit axis $\mathbf{n}$ can be described by the unit quaternion $q = [cos(\varphi/2), sin(\varphi/2)\mathbf{n}]$. The fixed vector $\mathbf{r}$ between the projection $\mathbf{r}^0$in the coordinate system O before rotation and the projection $\mathbf{r}^N$ of the coordinate system N after rotation can be expressed as:

$$\mathbf{r}^N = q^* \bigotimes \mathbf{r}^0 \bigotimes q \tag{5}$$

where $\mathbf{r}^0$ and $\mathbf{r}^N$ are two quaternion whose scalar part is 0 and vector part is $\mathbf{r}^0$ and $\mathbf{r}^N$, respectively; $q^* = [s, -\mathbf{v}]$ represents the conjugate quaternion, and the norm of a quaternion is defined as $\|q\| = q \bigotimes q^*$.

3. Three-dimension dynamic response tracking method

Acceleration is a physical quantity that is easy to obtain and relatively stable in the actual motion measurement of floating structures. Therefore, if a motion tracking model of floating structure can be constructed by combining acceleration and angular velocity, more stable and accurate results can be obtained as compared with the data by GPS. However, two main problems arise in solving this problem. The first is how to reconstruct the real dynamic response of the structure from the acceleration to mitigate the influence of the drift terms in the integration process caused by the unknown initial conditions, sensor baseline derivation and environmental noise. The second problem is how to better consider the impact of field test environment, equipment layout and tilt error of the used sensors on dynamic responses of floating structures.

3.1. Attitude calculation based on the quaternion

The basic idea of the quaternion method to determine the attitude of floating structures is to transform the orientation relationship between coordinate systems into the description of fixed-point rotation of rigid bodies, and the differential equation with respect to the quaternion is described as follows (Li et al., 2018):

$$\dot{Q}(t) = \frac{1}{2} Q(t) \bigotimes \omega_{ib} \tag{6}$$

where $Q = q_0 + q_1 i + q_2 k + q_3 j$, and ω_{ib} represents the angular velocity of the structure in the global coordinate system. Then, one can obtain:

$$\begin{bmatrix} \dot{q}_0 \\ \dot{q}_1 \\ \dot{q}_2 \\ \dot{q}_3 \end{bmatrix} = \frac{1}{2} \begin{bmatrix} 0 & -\omega_{ibx} & -\omega_{iby} & -\omega_{ibx} \\ \omega_{ibx} & 0 & \omega_{ibx} & -\omega_{iby} \\ \omega_{iby} & -\omega_{ibx} & 0 & \omega_{ibx} \\ \omega_{ibx} & \omega_{iby} & -\omega_{ibx} & 0 \end{bmatrix} \begin{bmatrix} q_0 \\ q_1 \\ q_2 \\ q_3 \end{bmatrix} \tag{7}$$

Therefore, the transformation matrix C_e from global coordinate system to dynamic coordinate system can be represented by quaternion as:

$$C_e = \begin{bmatrix} q_0^2 + q_1^2 + q_2^2 - q_3^2 & 2(q_1 q_2 + q_0 q_3) & 2(q_1 q_3 - q_0 q_2) \\ 2(q_1 q_2 - q_0 q_3) & q_0^2 - q_1^2 + q_2^2 - q_3^2 & 2(q_2 q_3 + q_0 q_1) \\ 2(q_1 q_3 + q_0 q_2) & 2(q_2 q_3 - q_0 q_1) & q_0^2 - q_1^2 - q_2^2 + q_3^2 \end{bmatrix} \tag{8}$$

And the relationship between quaternion and Euler angles can be obtained as:

$$\begin{aligned} \alpha &= -sin^{-1}(2 * (q_1 q_3 - q_0 q_2)) \\ \beta &= tan^{-1}(\frac{2(q_2 q_3 + q_0 q_1)}{q_0^2 - q_1^2 - q_2^2 + q_3^2}) \\ \theta &= tan^{-1}(\frac{2(q_1 q_2 + q_0 q_3)}{q_0^2 + q_1^2 + q_2^2 - q_3^2}) \end{aligned} \tag{9}$$

where α, β, and θ represent the dynamic Euler angles.

3.2. Tilt error correction of the measured acceleration

In the testing process, the measured data will contain a component of the gravitational acceleration as the rotation or tilt of the accelerometer occurs (Weng et al., 2017). Therefore, the tilt error in the measured acceleration is introduced as follows:

$$\boldsymbol{a}_s(t) = \boldsymbol{a}(t) + \boldsymbol{s}(t) \tag{10}$$

where the vector $\boldsymbol{a}(t) = [a_x(t) \;\; a_y(t) \;\; a_z(t)]$ represents the measured acceleration without the tilt error in the x, y and z directions, respectively. The item $\boldsymbol{s}(t)$ denots the tilt error.

Suppose a three-axis accelerometer, its static tilt error can be expressed as:

$$\boldsymbol{s}(t) = \boldsymbol{g} \quad for \quad \boldsymbol{\Phi}(t) = 0 \tag{11}$$

where $\boldsymbol{\Phi}(t) = [\alpha(t) \;\; \beta(t) \;\; \theta(t)]$, and $\boldsymbol{g} = [0 \;\; 0 \;\; -g]$ denotes the vector of gravitational accelerations of the Earth.

Then, the sensor is rotated with the angle of $\alpha(t)$, $\beta(t)$ and $\theta(t)$ around the x, y and z axes respectively. Based on the theory, the error of the accelerometer tilts can be expressed by the multiplication of the rotation matrices as:

$$\boldsymbol{s}(t) = \mathbf{R}(\boldsymbol{\Phi}(t))\boldsymbol{g} \tag{12}$$

where $\mathbf{R}(\boldsymbol{\Phi}(t))$ is composed of nine elements. Assume that angles are small, the equations $cos(\boldsymbol{\Phi}) \approx 1$, $sin(\boldsymbol{\Phi}) \approx \boldsymbol{\Phi}$ are satisfied. Therefore, $\mathbf{R}(\boldsymbol{\Phi}(t))$ can be defined as:

$$\mathbf{R}(\boldsymbol{\Phi}(t)) = \begin{bmatrix} 1 & 0 & 0 \\ 0 & 1 & -\alpha(t) \\ 0 & \alpha(t) & 1 \end{bmatrix} \begin{bmatrix} 1 & 0 & \beta(t) \\ 0 & 1 & 0 \\ -\beta(t) & 0 & 1 \end{bmatrix} \begin{bmatrix} 1 & -\theta(t) & 0 \\ \theta(t) & 1 & 0 \\ 0 & 0 & 1 \end{bmatrix} \tag{13}$$

Then, the tilt error can be rewritten into a vector-matrix form:

$$\boldsymbol{s}(t) = \boldsymbol{g}[-\beta(t) \quad \alpha(t) \quad -1]^T = \boldsymbol{g} + \begin{bmatrix} 0 & -1 & 0 \\ 1 & 0 & 0 \\ 0 & 0 & 0 \end{bmatrix} \boldsymbol{g}\boldsymbol{\Phi}(t) = \boldsymbol{g} + \mathbf{P}\boldsymbol{\Phi}(t) \tag{14}$$

And the acceleration without the tilt error can be written as:

$$\boldsymbol{a}(t) = \boldsymbol{a}_s(t) - \boldsymbol{g} - \mathbf{P}\boldsymbol{\Phi}(t) \tag{15}$$

It is noted that the tilt error of the accelerometer show in Eq. 15 can be eliminated once the Euler angle of the structure is determined. Moreover, the sensor should be installed away from the external interferences such as the high-frequency vibration equipment for the meaningful data, considering the environment conditions and safety considerations at the floating structure test site.

3.3. Acceleration decomposition and drift-caused term removal

Although there is a strict integration principle to describe the relationship between the acceleration and corresponding displacement of structures, the drift problem cannot be overcome by the direct integration technique due to the initial conditions, environmental noise and baseline deviation of sensor. Therefore, it is a challenging task to reconstruct the real displacement from the corrected acceleration without the effect of drift. To address this issue, the tilt-corrected acceleration a_x with the time interval Δt can be formulated as:

$$a_x = a_x(t_k) = \sum_{i=1}^{N_x} A_i e^{j\phi_n} e^{(-\xi_i\omega_i + j\omega_i\sqrt{1-\xi_i^2})k\Delta t} \tag{16}$$

where $t_k = k\Delta t$, $j = \sqrt{-1}$, $k = 0, 1, N_x - 1$, and N_x is the number of components in the sampled signal a_x. A, ξ, ω and ϕ represent the amplitude, damping ratio, natural frequency and phase of each component, respectively.

Then the Hankel matrix is introduced using equally-spaced discrete signals in the form of Eq. 17 (e.g.,) (Hu, et al., 2013):

$$\mathbf{H}_x(k) = \begin{bmatrix} a_{xk} & a_{x(k+1)} & \cdots & a_{x(k+N_c-1)} \\ a_{x(k+1)} & a_{x(k+2)} & \cdots & a_{x(k+N_c)} \\ \vdots & \vdots & \ddots & \vdots \\ a_{x(k+N_r-1)} & a_{x(k+N_r)} & \cdots & a_{x(k+N_r+N_c-2)} \end{bmatrix} \tag{17}$$

where N_r and N_c are the selected number of rows and columns to satisfy the equation $N_r + N_c + 1 = N$; $k = 0, 1, N - 1$, and N is the number of sampled signals.

Let the initial model order denoted as od equate to 2, and the singular value decomposition is applied to $\mathbf{H}_x(0)$ (Golub and Loan, 1996):

$$\mathbf{H}_x(0) = \begin{bmatrix} \mathbf{U}_{od}^x & \widetilde{\mathbf{U}}_{od}^x \end{bmatrix} \begin{bmatrix} \mathbf{S}_{od}^x & \mathbf{0} \\ \mathbf{0} & \mathbf{0} \end{bmatrix} \begin{bmatrix} (\mathbf{V}_{od}^x)^T \\ (\widetilde{\mathbf{V}}_{od}^x)^T \end{bmatrix} = \mathbf{U}_{od}^x \mathbf{S}_{od}^x (\mathbf{V}_{od}^x)^T \tag{18}$$

where $\mathbf{U}_{od}^x$, $\mathbf{S}_{od}^x$ and $\mathbf{V}_{od}^x$ are singular vectors with a dimension of $N_r \times od$, $od \times od$ and $N_r \times od$, respectively.

Then, a relationship between $\mathbf{H}_x(0)$ and $\mathbf{H}_x(1)$ can be determined in Eq. 19:

$$\mathbf{H}_x(1) = \mathbf{U}_{od}^x \sqrt{\mathbf{S}_{od}^x} \mathbf{A} \sqrt{\mathbf{S}_{od}^x} (\mathbf{V}_{od}^x)^T \tag{19}$$

where $\mathbf{A} = e^{\mathbf{F}\Delta t}$, and $\mathbf{F}$ is a similarity transformation of a coefficient matrix of a converted first-order matrix differential equation.

In addition, a stopping criterion SC_{sw} is defined to improve the accuracy of the decomposition as:

$$SC_{sw} = |\frac{|S_x^{od+2}| - |S_x^{od}|}{S_x^{od}}| \tag{20}$$

where $|\ |$ means the absolute value of a number. S_x^{od} are values of the power spectral density function as:

$$S_x^{od} = max[20 \log_{10}(S_x^{od}(\omega))] \tag{21}$$

where $max[\cdot]$ means the maximum value. Using the above method to iteratively extract the maximum energy component for the construction of the acceleration, one has:

$$a_x(t) = \sum_{i=1}^{N_x} A_i e^{j\phi_i} e^{(-\xi_i\omega_i + j\omega_i\sqrt{1-\xi_i^2})t} = \sum_{i=1}^{N_x} \gamma_i e^{\lambda_i t} \tag{22}$$

where $\gamma_i = A_i e^{j\phi_i}$ and $\lambda_i = -\xi_i\omega_i + j\omega_i\sqrt{1-\xi_i^2}$ represent the decomposed complex exponential parameters.

Then, the tilt-corrected accelerations can be expressed in the form of complex exponential sequences shown in Eq. 23:

$$\boldsymbol{a}(t) = [a_x(t)\ \ a_y(t)\ \ a_z(t)] = [\sum_{i=1}^{N_x}\gamma_x e^{\lambda_x t}\ \ \sum_{i=1}^{N_y}\gamma_y e^{\lambda_y t}\ \ \sum_{i=1}^{N_z}\gamma_z e^{\lambda_z t}] \tag{23}$$

where λ and γ represent the complex exponential parameters of the corrected acceleration in the corresponding direction. N_y and N_z are the numbers of components in the sampled signal a_y and a_z, respectively. More detailed information about the complex exponential decomposition of accelerations can be found in Liu et al. (2020) and Gao et al. (2021).

3.4. Displacement reconstruction and three-dimension motion tracking

Once the complex exponential sequence representing the acceleration has been obtained, the components of structural accelerations can be screened and removed using Eq. 24:

$$f_x = \frac{imag(\lambda_x)}{2\pi} \tag{24}$$

where $imag$ means the value's imaginary part. After the frequency of each component is obtained, the drift-caused term can be accurately eliminated by setting a screening criteria as

$$\begin{cases} f_x > F, Reconstruction\ for\ displacement \\ f_x < F, Needs\ to\ be\ eliminated \end{cases} \tag{25}$$

where F is set artificially, usually less than the structural frequency of motion, and slightly greater than 0. After removing the drift-caused terms, the components corresponding to the remaining frequencies f_x are the real components of the structural motion which can be determined by λ_x and γ_x corresponding to the f_x.

Then, the remaining part of components of structural accelerations can be reconstructed by Eq. 26:

$$\widetilde{\boldsymbol{a}}(t) = [\widetilde{a}_x(t)\ \ \widetilde{a}_y(t)\ \ \widetilde{a}_z(t)] = [\sum_{i=1}^{\widetilde{N}_x}\widetilde{\gamma}_x e^{\widetilde{\lambda}_x t}\ \ \sum_{i=1}^{\widetilde{N}_y}\widetilde{\gamma}_y e^{\widetilde{\lambda}_y t}\ \ \sum_{i=1}^{\widetilde{N}_z}\widetilde{\gamma}_z e^{\widetilde{\lambda}_z t}] \tag{26}$$

where $\widetilde{N}_x$, $\widetilde{N}_y$, and $\widetilde{N}_z$ represent the number of remaining components in the signal $\widetilde{a}_x(t)$, $\widetilde{a}_y(t)$ and $\widetilde{a}_z(t)$ after removing the drift-caused terms. $\widetilde{\gamma}$ and $\widetilde{\lambda}$ represent the remaining complex exponential sequences

in corresponding directions. $\widetilde{a}_x(t)$, $\widetilde{a}_y(t)$ and $\widetilde{a}_z(t)$ represent the reconstructed acceleration without drift-caused terms in three directions, respectively.

Taking the acceleration $\widetilde{a}_x(t)$ as an example, Eqs. 27 and 28 can be obtained by the integration on both sides of Eq. 26 with respect to t:

$$\begin{cases} v_x(t) = \int_0^t \widetilde{a}_x(t)dt + v_x(0) \\ x(t) = \int_0^t \int_0^t \widetilde{a}_x(t)dtdt + v_x(0)t + x(0) \end{cases} \tag{27}$$

$$\begin{cases} \int_0^t \widetilde{a}_x(t)dt = \sum_{i=1}^{\widetilde{N}_x} \{\frac{\widetilde{\gamma}_x}{\widetilde{\lambda}_x} e^{\widetilde{\lambda}_x t} - \frac{\widetilde{\gamma}_x}{\widetilde{\lambda}_x}\} \\ \int_0^t \int_0^t \widetilde{a}_x(t)dtdt = \sum_{i=1}^{\widetilde{N}_x} \{\frac{\widetilde{\gamma}_x}{\widetilde{\lambda}_x^2} e^{\widetilde{\lambda}_x t} - \frac{\widetilde{\gamma}_x}{\widetilde{\lambda}_x^2}\} \end{cases} \tag{28}$$

By comparison of these two equations, the real dynamic displacement $x(t)$ and initial displacement $x(0)$ can be estimated as:

$$\begin{cases} v(t) = \sum_{i=1}^{\widetilde{N}_x} \frac{\widetilde{\gamma}_z}{\widetilde{\lambda}_z} e^{\widetilde{\lambda}_z t} \\ v(0) = \frac{\widetilde{\gamma}_z}{\widetilde{\lambda}_z} \end{cases} \tag{29}$$

and

$$\begin{cases} x(t) = \sum_{i=1}^{\widetilde{N}_x} \frac{\widetilde{\gamma}_z}{\widetilde{\lambda}_z^2} e^{\widetilde{\lambda}_z t} \\ x(0) = \frac{\widetilde{\gamma}_z}{\widetilde{\lambda}_z^2} \end{cases} \tag{30}$$

Similarly, the other two displacement components can be reconstructed:

$$[x(t) \;\; y(t) \;\; z(t)] = [\sum_{i=1}^{\widetilde{N}_x} \frac{\widetilde{\gamma}_x}{\widetilde{\lambda}_x^2} e^{\widetilde{\lambda}_x t} \quad \sum_{i=1}^{\widetilde{N}_y} \frac{\widetilde{\gamma}_y}{\widetilde{\lambda}_y^2} e^{\widetilde{\lambda}_y t} \quad \sum_{i=1}^{\widetilde{N}_z} \frac{\widetilde{\gamma}_z}{\widetilde{\lambda}_z^2} e^{\widetilde{\lambda}_z t}] \tag{31}$$

where $x(t)$, $y(t)$ and $z(t)$ are the reconstructed dynamic displacement corresponding to the measured acceleration. Furthermore, since the reconstructed displacement is the motion at the test point, it needs to be transformed to the COG through coordinate transformation:

$$\begin{bmatrix} x_G(t) \\ y_G(t) \\ z_G(t) \end{bmatrix} = \mathbf{T} \begin{bmatrix} \bar{x} \\ \bar{y} \\ \bar{z} \end{bmatrix} + \begin{bmatrix} x(t) \\ y(t) \\ z(t) \end{bmatrix} + \begin{bmatrix} x_0 \\ y_0 \\ z_0 \end{bmatrix} \tag{32}$$

where $[x_G(t) \;\; y_G(t) \;\; z_G(t)]^T$ represents the dynamic displacement at the COG, $[x_0 \;\; y_0 \;\; z_0]^T$ includes the coordinate of the measured point in the global coordinated system, $[\bar{x} \;\; \bar{y} \;\; \bar{z}]^T$ is the position of the measured point relative to the COG of the structure in the dynamic coordinate system, and $\mathbf{T}$ denotes the transformation matrix shown in Eq. 2.

With Euler angle defined by Eq. 9, the model with 6-DOF motions including the acceleration and angular velocity information has been established, and the motion tracking system to effectively position the floating structures has been realized.

3.5. Establishment of 6-DOF motion tracking system

The procedure of the proposed approach to the positioning of ocean floating structures can be described as follows. Firstly, the motion attitude is determined by the quaternion method, and subsequently the tilt error and installation position of the sensor are corrected using the estimated Euler angle. Following that, the displacement reconstruction model of the floating structure is established in the form of complex exponential sequences. Based on the reconstructed displacement and estimated Euler angle, a 6-DOF motion tracking system is finally developed.

The procedure of the proposed approach to the positioning of marine floating structures can be described by five steps as follows:

- Step 1 - Euler angle estimation and tilt correction: The angular velocity measured by the gyroscope is substituted into Eq. 6 to update the quaternion for the correction of the dynamic Euler angle using Eq. 9; Due to the rotation of accelerometers, the tilt error is evaluated using Eq. 14, and the acceleration is corrected by Eq. 15;

- Step 2 - Decomposition of corrected acceleration: The acceleration is represented in the form of Eq. 16, and a relationship between the Hankel matrix H(0) and H(1) is established as Eqs. 17 and 19, and the acceleration is finally expressed using complex exponential sequences defined by Eq. 23,

- Step 3 - Drift-caused removal and displacement reconstruction: A screening criteria is set using Eq. 25 for the elimination of the drift-caused term, and the remaining sequence is substituted into Eq. 27 for displacement reconstruction.

- Step 4 - Realization of 6-DOF tracking system: The calculated Euler angle is substituted into Eq. 2 to solve the transformation matrix T. Substituting the reconstructed displacement, the solved matrix T, and the relative coordinates of the measured point and the COG position into Eq. 32, the reconstructed displacement is converted to the position in the COG system of the structure. By combining the Euler Angle calculated by Eq. 9 with the dynamic displacement estimated by Eq. 31, a 6-DOF motion tracking system is realized to position the marine floating structures.

The flowchart of this novel motion tracking system has been shown in Fig. 2.

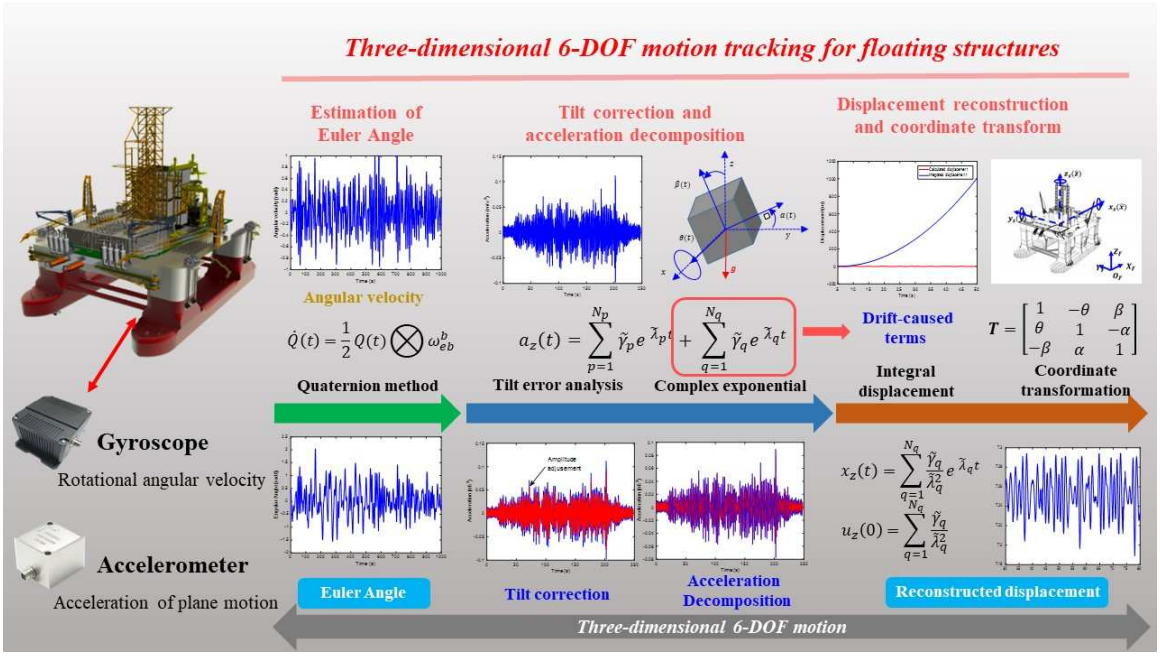

Fig. 2: The flowchart of the proposed method.

4. Numerical example: An SDOF floating system

To demonstrate the calculation process and verify the correctness of the proposed approach to the motion tracking of floating structures, an SDOF model to simulate the floating system has been investigated in this section. To realize the measured acceleration, the artificially baseline offset and signal truncation have been applied to the acceleration obtained by the Newmark-β method for the displacement reconstruction. On this basis, effects of the sensor tilt on the accuracy of the reconstructed displacement have been discussed.

4.1. Simulation and decomposition of measured acceleration

Based on the linear theory, the Cummins equation (Cummins, 1962) was introduced to simulate the movement process of the SDOF floating structures as follows:

$$(m + m_a)\ddot{x}(t) + \int_0^t K(t-\tau)\dot{x}(\tau)d\tau + cx(t) = F(t) \tag{33}$$

where m, m_a and c represent the structural mass, the additional mass and the restoring coefficient, respectively. $\ddot{x}(t)$, $\dot{x}(t)$ and $x(t)$ denote the acceleration, velocity and displacement of the system under the excitation force $F(t)$; $K(t-\tau)$ depicts the influence of the momentum change of the fluid at a particular moment on the motion at subsequent moment and is mathematically expressed as:

$$K(t) = (1+\nu)e^{-\nu t}[cos(\nu t) - \frac{\mu}{\nu}sin(\nu t)] \tag{34}$$

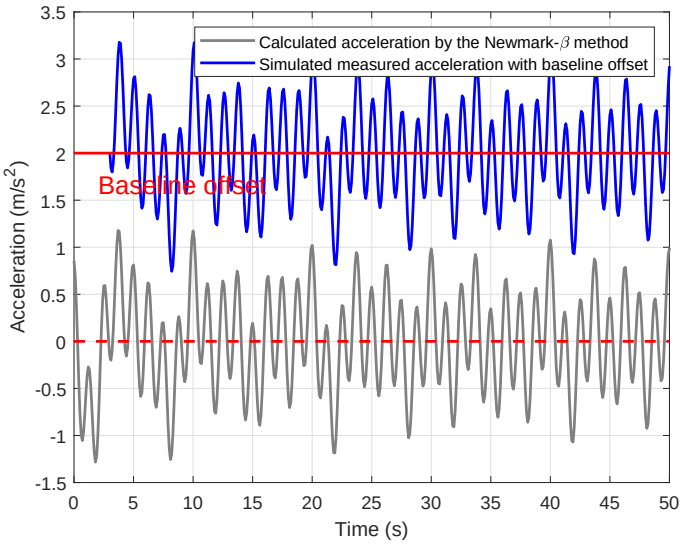

Fig. 3: The calculated acceleration and simulated acceleration.

As the motion response of the structure is mainly concerned in this section, only a simple model is adopted here to study the correctness of the proposed method applicable to floating structures. Assume that a representative model with the parameters including $m = 1$kg, $c = 5.5$N/m, $\mu = 0.2$ and $\nu = 2$ in Eq. 33 and 34 has been considered as a numerical SDOF example. The force $F(t)$ has been defined by Eq. 35:

$$F(t) = \sum_{n=1}^{3} A_n e^{-\xi_n t_k} cos(2\pi f_n t_k + \theta_n) \tag{35}$$

where $A_n = [1.2, 0.2, 0.8]$m, $f_n = [0.3, 0.2, 0.8]$Hz, $\theta_n = [-\pi/4, \pi/8, 0]$ and $\xi = [0, 0, 0]$.

The acceleration of the SDOF model calculated by the Newmark-β method has been shown in Fig. 3, where the initial velocity and initial displacement are set to 0.5m/s and 0.2m in the calculation with the time step $\Delta t = 0.1s$. As the acceleration acquired by sensors usually contains the baseline component and the initial conditions of the structure during the measurement, which are usually unknown, will lead to the drift of the displacement when the displacement is obtained using the direct integration of the acceleration. Taking into account the aforementioned situations encountered by the structure in a more realistic environment, the truncation (starting from 3s) and the baseline offset $\delta = 2$ have been applied to the calculated acceleration by the Newmark-β method, as the input signal, for displacement reconstruction in the following section. The acceleration result by the Newmark-β method has been compared with the simulated acceleration in Fig. 3.

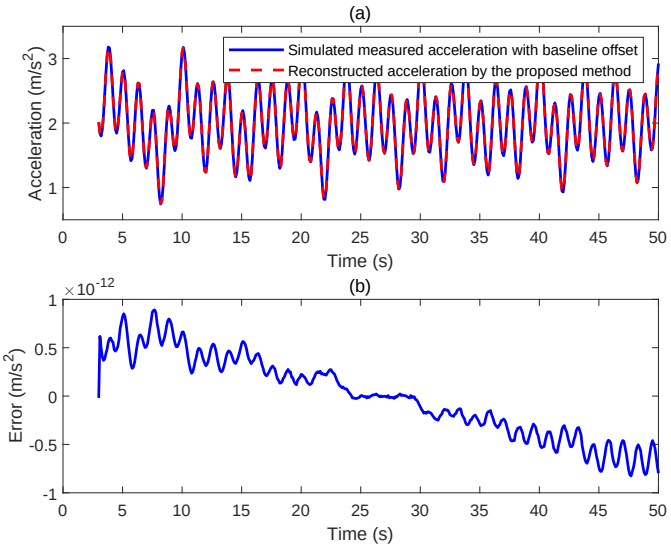

Fig. 4: The comparison of (a) the decomposed and simulated acceleration; (b) the reconstructed error.

To reconstruct the displacement of the system, the complex exponential sequence has been applied to decompose the acceleration in the first instance. By setting the extraction value of 6 in the decomposition process, six pairs of $\widetilde{\lambda}_m$ and $\widetilde{\gamma}_m$ have been obtained for the reconstruction of the acceleration shown in Fig. 4 (a) and the error between the reconstructed acceleration and the acceleration by the Newmark-β method has been provided in Fig. 4 (b). It is noted that the reconstructed acceleration has been in good agreement with the results by the Newmark-β method, which proves that the decomposed complex exponential sequences can characterize the original acceleration with a high level of precision.

4.2. Displacement reconstruction based on simulated acceleration

Moreover, the frequency of each component $f_m = [0\text{Hz}\ 0.2\text{Hz}\ 0.2195\text{Hz}\ 0.3\text{Hz}\ 0.4403\text{Hz}\ 0.8\text{Hz}]$ has been estimated based on $\widetilde{\lambda}_m$. It can be observed that the acceleration includes both the steady response caused by the external force (0.2Hz, 0.3Hz and 0.8Hz) and the transient response due to the initial velocity and displacement (0.2195Hz and 0.4403Hz) as well as the base line offset of the sensor (0Hz). The responses of the decomposed components in the time domain have been shown in Fig. 5.

On the completion of the acceleration decomposition, the component which causes the displacement drift ($f_m = 0$) can be accurately separated, and then the remaining data used to reconstruct the velocity and displacement of the system will be obtained. The results by the Newmark-β method, the reconstructed velocity and displacement have been presented in Fig. 6. It has been observed that the reconstructed velocity

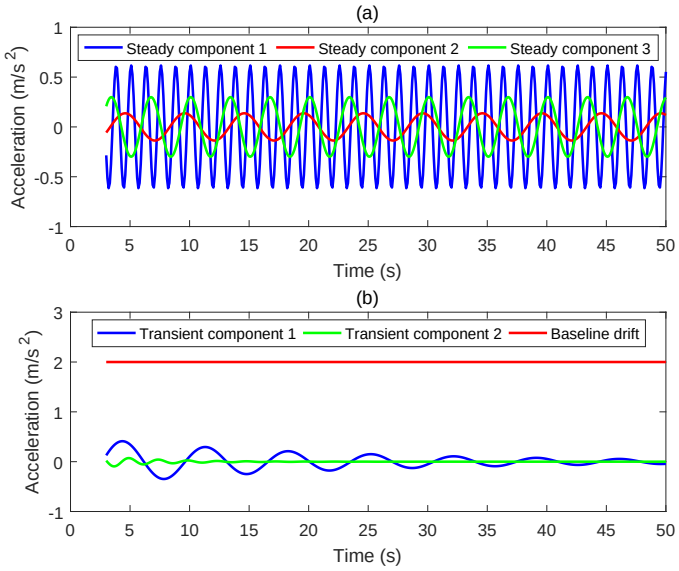

Fig. 5: The decomposed (a) steady components; (b) transient components and drift term.

and displacement have been accurately achieved as the results have been slightly affected by the baseline offset and the initial conditions of the system due to the non-integral drift-free mechanism of the proposed method.

5. Numerical example: A semi-submersible platform

To further verify the feasibility of the proposed approach to the response tracking of floating structures, a numerical example of a semi-submersible platform modeled by the Orcaflex has been conducted to obtain the 6-DOF motion responses under the consideration of regular and irregular waves. Following that, comparison results of the motion tracking between the proposed approach and Orcaflex have been discussed.

5.1. Model introduction and measuring point setting

The semi-submersible platform is composed of a buoy and columns shown in Fig. 7. It is dimensioned with the length, width and height of 82m, 71.2m and 70m, respectively. The mooring system is divided into four groups, each of which includes three cables. In Fig. 8, four groups of cables are symmetrically distributed regarding the x and y axes. The coordinates for the fairleads and the fixed points at the seabed are labeled. Detailed parameters of the platform and the properties of the mooring line have been provided in Table 1.

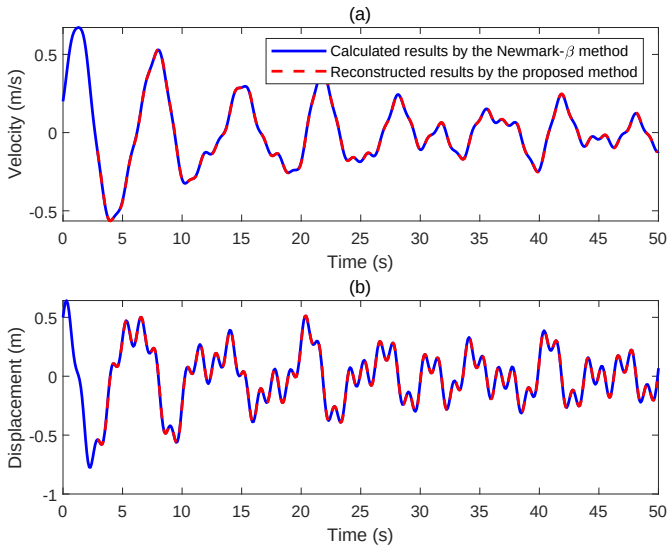

Fig. 6: The comparison of the calculated and reconstructed (a) velocity and (b) displacement.

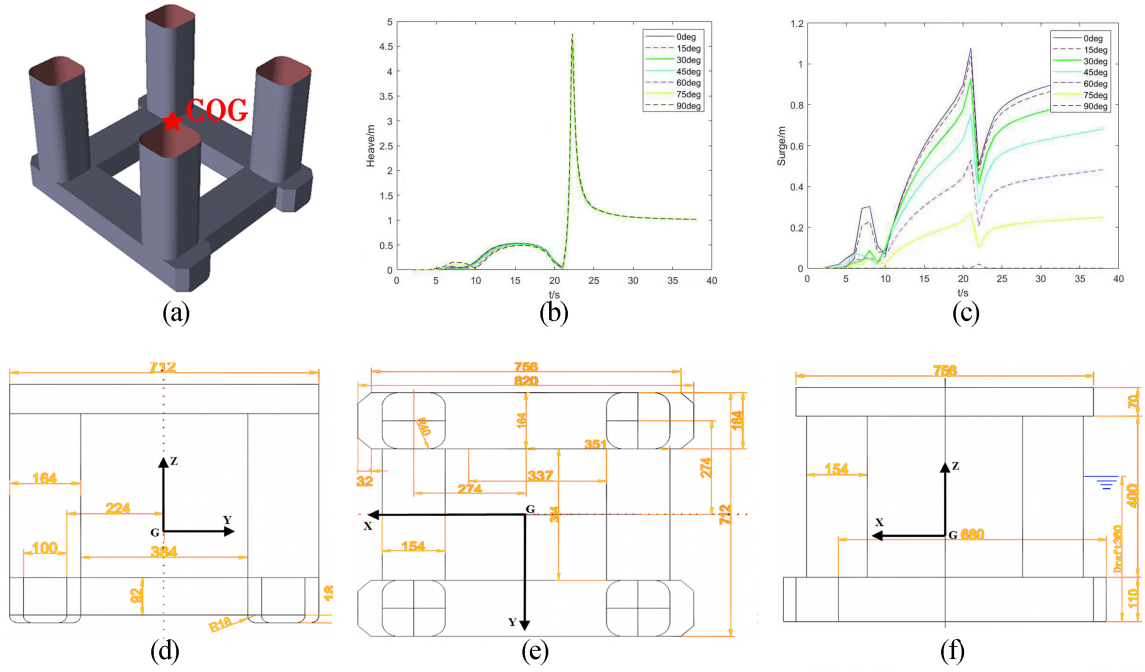

Fig. 7: Drawings of the platform: (a) Hull surfaces, RAOs in the (b) Heave and (c) Surge direction, and (d) front, (e) side, (f) top view.

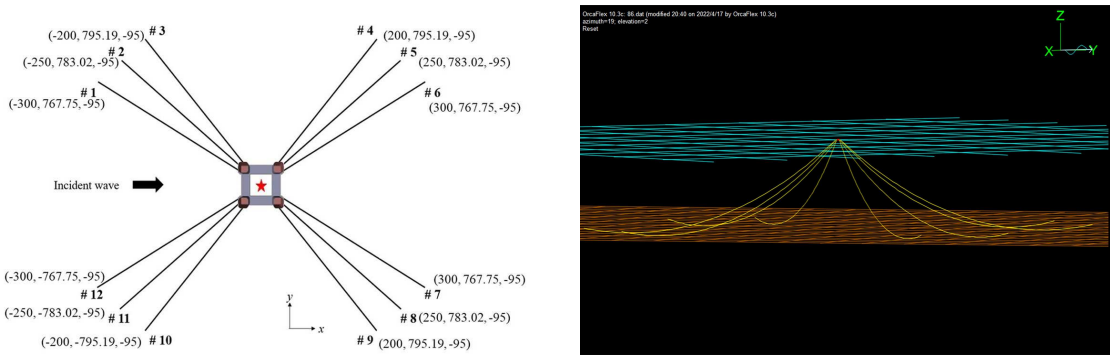

(a) (b)

Fig. 8: (a) The numerical model of the mooring layout; (b) The catenary curve for the mooring lines at the pretension condition.

Table 1: Parameters of the numerical platform and mooring system.

Platform			Mooring system		
Item	Value	Unit	Item	Value	Unit
Draft	36	m	Equivalent diameter	0.149	m
Displacement	65700	m^3	Dry weight per unit length	7397.824	N/m
Radii of gyration	22.8/23.2/23.2	m	Wet weight per unit length	6436.43	N/m
COG from keel	21.88	m	Axial stiffness (Giovanni et al., 2022)	641000000	$N{\cdot}m^2$
Waterline area	955	m^2	Bending stiffness	18	$N{\cdot}m^2$

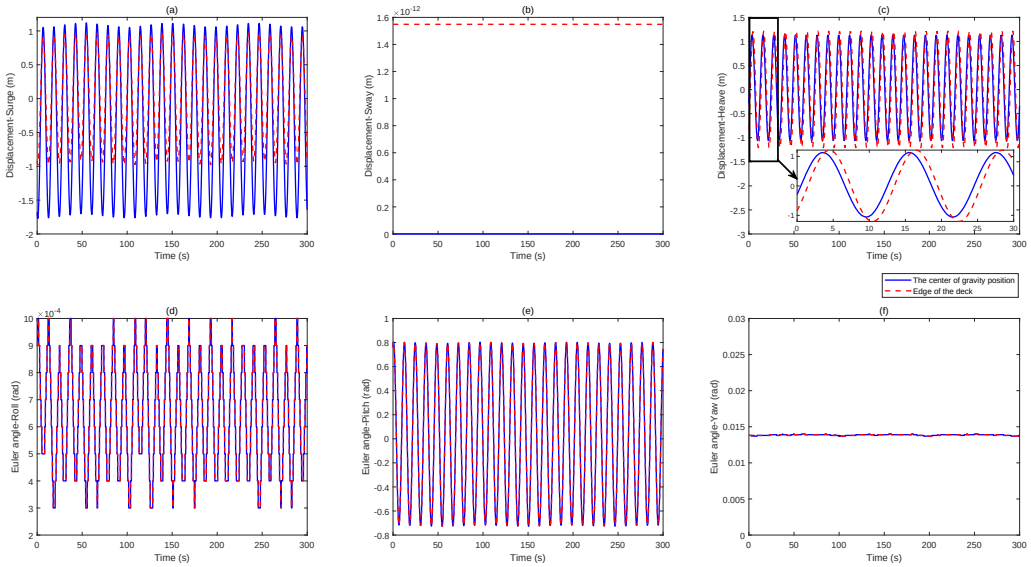

Fig. 9: The comparison of the calculated 6-DOF motion at the COG and point (41m, -35m, 35m) in the (a) surge, (b) sway, (c) heave, (d) roll, (e) pitch and (f) yaw directions.

5.2. Influence of different test points on motion response

Due to the limitations of the site environment and equipment installation, it is challenging to directly measure the acceleration at the COG of the structure, leading to the position error in the measuring process. To overcome this issue, the measurement of the acceleration has to be transformed to the COG in the analysis. It has been worth noting that the acceleration and angular velocity at the location (41m, -35m, 35m) of the deck edge have been referred in this example to track the 6-DOF motion of the structure. In Fig. 9, the 6-DOF motion responses at the reference position and the COG have been presented considering the action of regular wave with the wave height of 8m and the period of 12s.

It has been observed that the main difference of structural response at different positions lies in the amplitude of dynamic displacement as shown in Figs. 9 (a) and (c). At the same time, the change of the heave motion at different positions has occurred in both amplitude and phase shown in Fig. 9 (e) and the rotational motion is consistent (as shown in Figs. 9 (b), (d) and (f)), indicating that the Euler angle at any position can be used to correct the tilt error and transform the corrected acceleration to the COG of the structure.

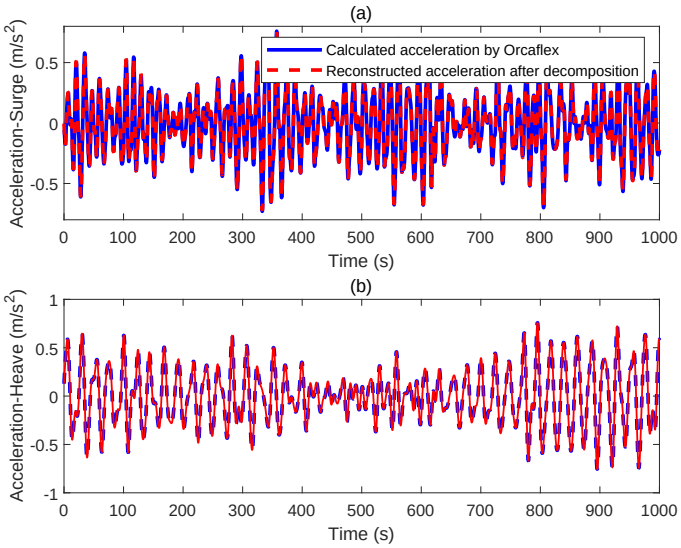

Fig. 10: The comparison of the calculated, transformed, and reconstructed acceleration in the (a) surge and (b) heave direction.

5.3. Three-dimension dynamic response tracking under irregular waves

To examine the feasibility of the proposed method for tracking the 6-DOF motion of floating structures subject to uncomplicated sea conditions, irregular waves with the wave height of 10m and the period of 12s (simulated by Jonswap spectrum) have been applied to excite the platform. Similarly, the motion responses at the COG of the structure and the referred position (41m, -35m, 35m) at the deck have been calculated. As there is no sensor tilt error in the calculation results by Orcaflex, the decomposition of acceleration can be carried out directly. With the extracted number 450 and 200 in the surge and heave direction, and $SC_{sw} = 1 \times 10^{-3}$, the corrected acceleration in the proposed tracking approach has been decomposed. Results in Figs. 10 and 11 have shown that the reconstructed accelerations are consistent with the simulation results with a high level of precision, which proves the correctness of decompose sequences for the displacement reconstruction.

Then, the drift-caused components with frequencies approaching 0Hz can be removed, where the first 33 components in the surge direction and the first 11 components in heave direction. And the remaining sequences used to reconstruct corresponding displacements have been shown in Fig. 12. In addition, Fig. 13 compares the two displacement results in the frequency domain, and it can be seen that the reconstructed displacements has well agreed with the results by Orcaflex both in the time and frequency domains. Once the Euler angle and linear displacement of the structure are achieved, the coordinate transformation of

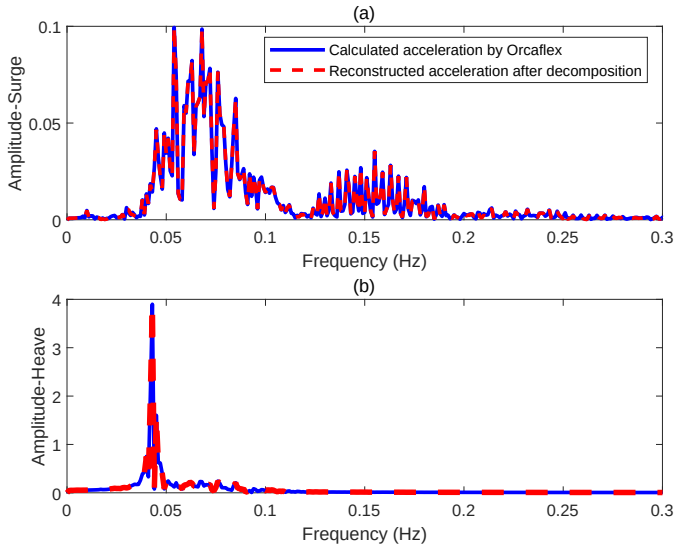

Fig. 11: The comparison of the calculated, transformed, and reconstructed acceleration in the frequency domain in the (a) surge and (b) heave direction.

acceleration can be carried out. And in the analysis, the Euler angle has been solved by the quaternion method using the calculated angular velocity and the reconstructed displacement has been transformed to the COG system of the structure.

Once the dynamic displacement and Euler angle of the structure is obtained, the 6-DOF motion response of the structure will be determined. Considering the wave action, the tracking motion of the platform at 209.40s and 254.30s have been shown in Fig. 14 (a) and (b), respectively. It has been observed that the reconstruction results have well agreed with the simulations by Orcaflex. The correctness of the proposed method to track the 6-DOF motion of floating structures has been demonstrated by the maximum reconstruct error of 0.8096%. It is worth noting that the error of the motion posture in the roll direction of 293.5s reaches 16.6667%, this is because that the motion amplitude of the structure at this moment in the roll direction is small (only 0.0006 rad), and in this case, even small differences can cause large errors.

6. Experimental example: A semi-submersible platform

To validate the correctness of the developed approach from the experimental point of view, a laboratory test of the semi-submersible platform in Fig. 7 has been carried out to track the 6-DOF motion with the comparison of the measured results by the optical tracking system.

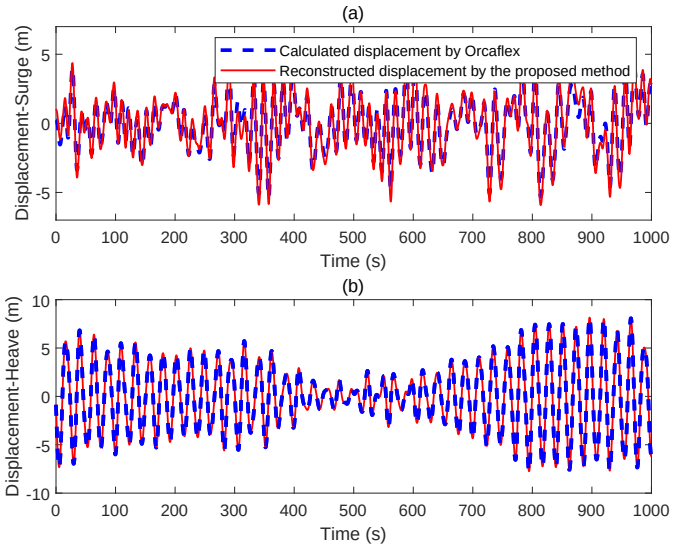

Fig. 12: The comparison of the reconstructed and calculated displacement in the (a) surge and (b) heave direction.

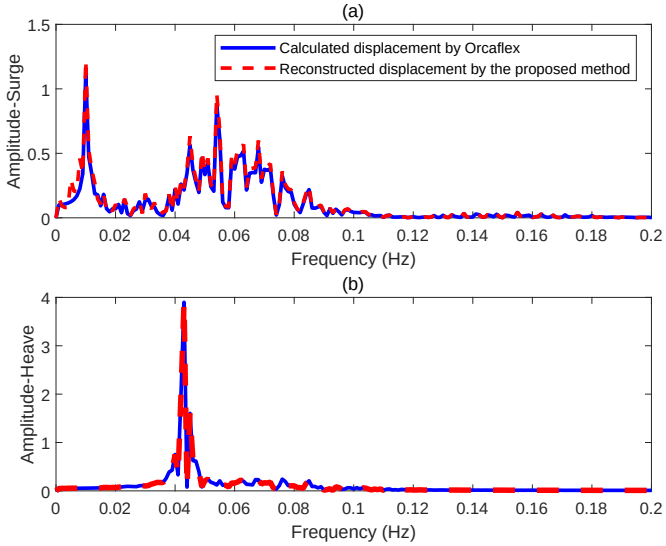

Fig. 13: The comparison of the reconstructed and calculated displacement in the frequency domain in the (a) surge and (b) heave direction.

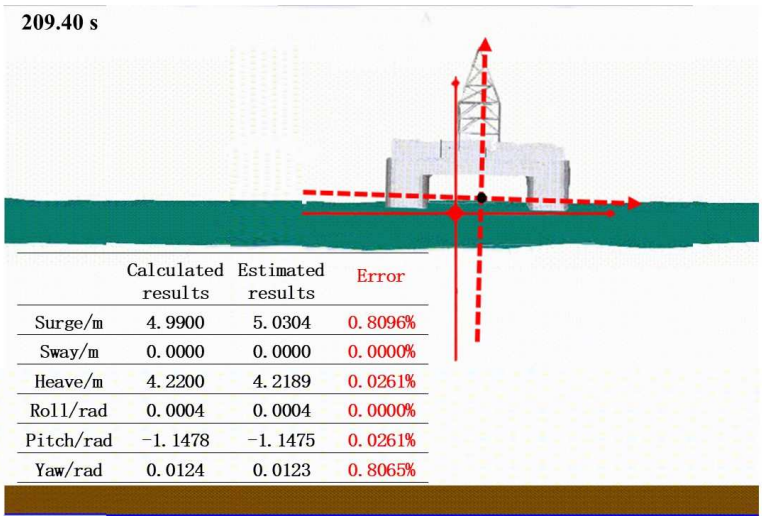

	Calculated results	Estimated results	Error
Surge/m	4.9900	5.0304	0.8096%
Sway/m	0.0000	0.0000	0.0000%
Heave/m	4.2200	4.2189	0.0261%
Roll/rad	0.0004	0.0004	0.0000%
Pitch/rad	−1.1478	−1.1475	0.0261%
Yaw/rad	0.0124	0.0123	0.8065%

(a)

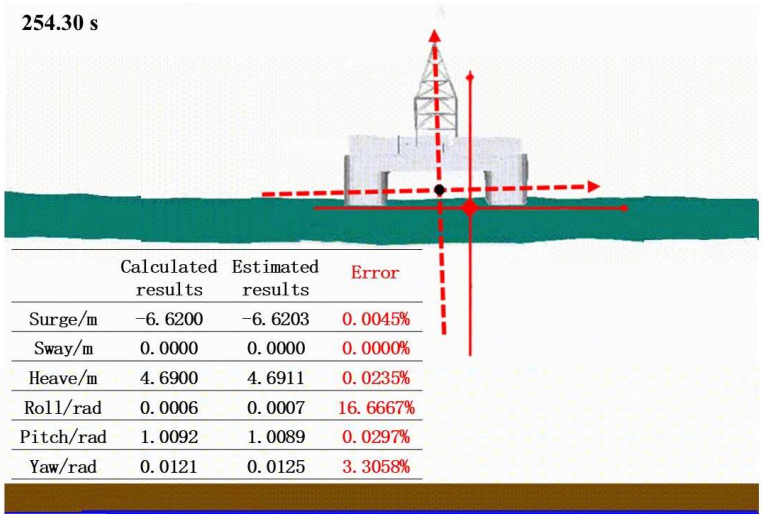

	Calculated results	Estimated results	Error
Surge/m	−6.6200	−6.6203	0.0045%
Sway/m	0.0000	0.0000	0.0000%
Heave/m	4.6900	4.6911	0.0235%
Roll/rad	0.0006	0.0007	16.6667%
Pitch/rad	1.0092	1.0089	0.0297%
Yaw/rad	0.0121	0.0125	3.3058%

(b)

Fig. 14: 6-DOF motion tracking results at (a) 209.40s, and (b) 254.30s of the platform under irregular waves.

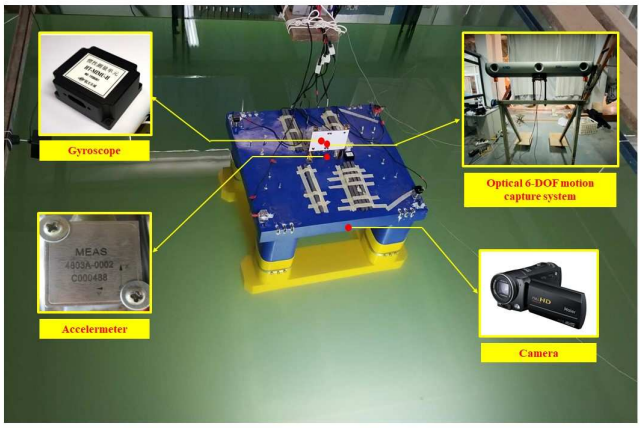

Fig. 15: The physical model of the platform and sensor arrangement.

6.1. Brief Introduction to the experimental setup

A 1:100 model has been established to represent the semi-submersible platform using the parameters shown in Fig. 15. The mooring cable which the properties including a pretension of 100g (which is a certain amount of stress applied to the mooring structure in advance, so that the structure has an ability to resist the normal deformation), a dry weight of 332.28g/m, an equivalent diameter of 0.00149m, and an elongation of 3.5cm/kg in the experiment has composed of pure steel wires and springs. Model experiments are conducted in the wave flume (60m $\times$ 3m) of the Ocean University of China and the water depth is kept at 1m. The piston type generator is fixed at the end of the wave flume.

In the experiment, the accelerometer and gyroscope are installed on the platform. The accelerometer used is a three-axis accelerometer produced by SILICON DESIGNS, Inc., model MEAS 4803A002-000488. Its ranges for the frequency response and voltage are denoted as 0-800Hz and 0.5-4.5V, respectively. Also, the voltage sensitivity is 200mV/g. The gyroscope used is HT-IMU-500, which incorporates a three-axis high-precision MEMS gyroscope with zero offset stability of 0.1 to $3^o/\text{h}$. In addition, a 16-channels IMC acquisition instrument has been used to collect the acceleration and angular velocity of the structure. To obtain the true motion of the structure, a camera and a non-contact optical tracking system have been mounted on one side of the pool. The optical system contains three positioning sensors, with a maximum sampling frequency of 4600Hz and a test resolution of 0.01mm. The equipment and layout in the test have been shown in Fig. 15. More detailed information about the experiment can be found in Yu et al. (2022).

6.2. *Three-dimension dynamic response tracking under regular waves*

Considering regular waves with the wave height of 0.06m and the period of 2.8s, Fig. 16 has shown the measured Euler angle in three rotational directions and the linear acceleration in three translational directions of the structure. It has been noted that the structure starts to move at 17s under the action of waves and tends to be stable after 30s. The reason for this phenomenon owes to the fact that the initial stage of the structure motion is a typical unsteady response, which does not conform to the rule of the motion of structures subject to the action of regular waves. With the increase of time, the motion of the platform gradually stabilizes and stops after 150s. Therefore, in the following analysis, the response in the relative stable stage of the structural motion (between 60s to 120s) has been selected for data analysis. Due to the baseline deviation of the sensor, the average values of the measured acceleration in the three directions are different.

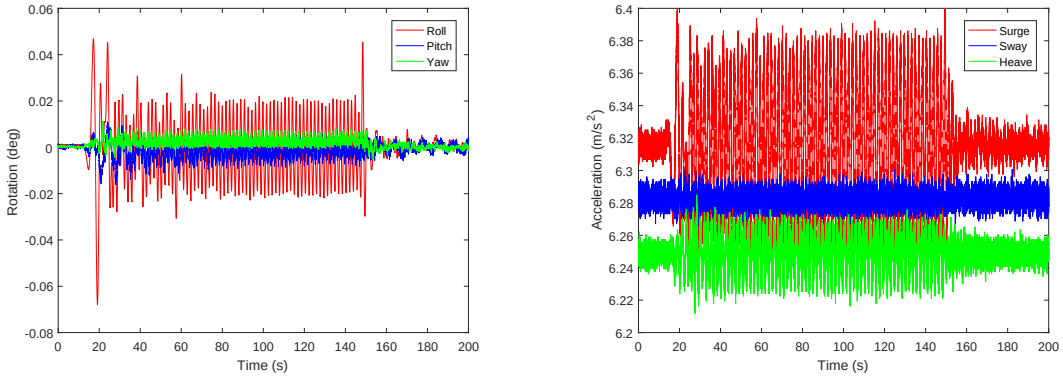

(a) (b)

Fig. 16: The (a) estimated Euler angle and (b) measured acceleration of the platform under regular waves.

To track the structural motion, the tilt errors should be corrected initially. Figure 17 has shown the corrected acceleration in the directions of surge and heave of the structure. In the decomposition of the corrected acceleration, SC_{sw} is set to 1×10^{-3} and the extracted number are set as 1200 and 1800 as the response in surge direction is often more complex than that in heave direction. Results have shown that the accelerations in both the surge and heave directions have been well reconstructed to represent the original measured accelerations.

On the completion of the decomposition process, the components whose frequencies close to 0Hz have been removed in order to reconstruct the corresponding displacement. In this case study, the first 23 components and 62 components in the heave and surge directions have been removed. Then, the reconstructed

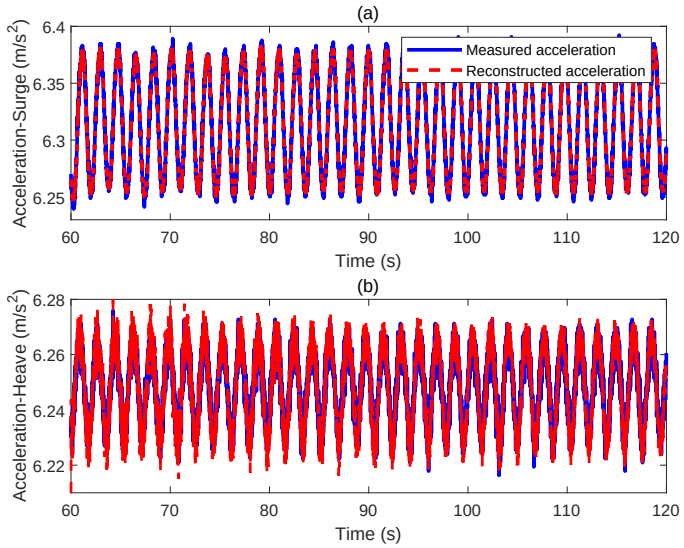

Fig. 17: The comparison of the measured and reconstructed acceleration in the (a) surge and (b) heave direction.

displacements are transformed to the COG of the structure, and results in Fig. 18 have shown that the reconstructed displacement has well agreed with the measured results by the optical tracking device, which has indicated that the proposed approach has the ability to reconstruct the dynamic displacement of floating structures under regular waves. With the combination of rotational Euler angle obtained by the quaternion method, the structural motion has been successfully tracked in Fig. 19. The tracking motions including the positions at the moment when the structure begins to move (0.00s) and two moments of 97.4870s and 104.8870s have been given. It has been noted that the results have been consistent with the images taken by the camera, which has recorded the operation state of the structure. Also, the comparison of results by the proposed approach with the data by the optical tracking device have been provided in Table 2. Since the optical system adopts non-contact measurement method and usually has high accuracy which can up to 0.0001mm, the measured results are taken as the standard results, and expressed as ”Measured results”, and ”Estimated results” in the table represents the results estimated by the proposed method. The comparison has indicated that the proposed approach has the ability to track the motions of structures with a high level of accuracy. Furthermore, the estimated errors of the tracking system in the sway and pitch directions are slightly large as the structural movements in the two directions theoretically approach to zeros due to the incident wave with 180 degrees and even a tiny movement can lead to a noticeable error.

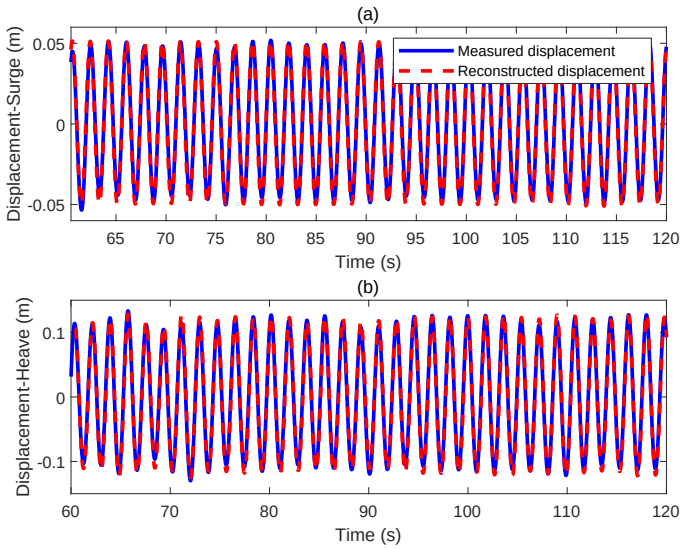

Fig. 18: The comparison of the measured and reconstructed displacement in the (a) surge and (b) heave direction.

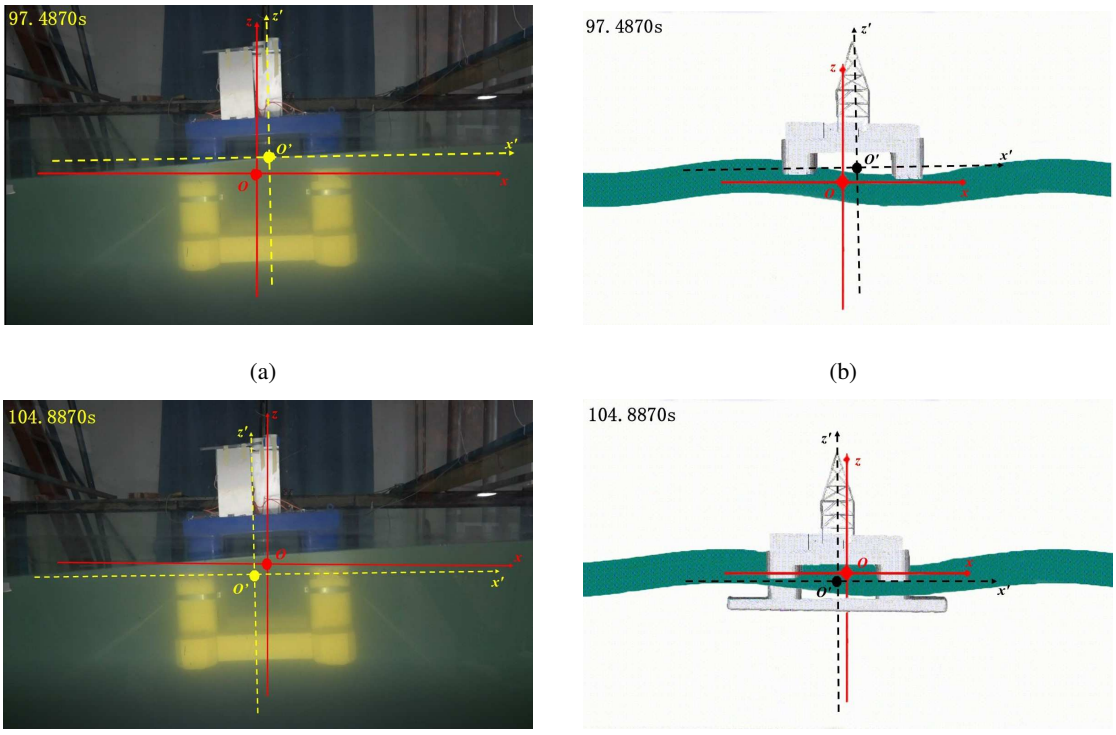

Fig. 19: The comparison results of the platform under regular waves between (Left) camera and (Right) the proposed method: (a) and (b) t=97.4870s; (c) and (d) t=104.8870s.

Table 2: 6-DOF motion tracking values of the platform under regular waves.

Time	97.4870s			104.8870s		
	Measured results	Estimated results	Error	Measured results	Estimated results	Error
Surge (mm)	49.3447	49.3378	-0.0140%	-36.6124	-36.6135	0.0030%
Sway (mm)	0.0080	0.0073	-8.7500%	4.9936	4.9910	0.0521%
Heave (mm)	63.6563	63.6563	0.0000%	-24.9672	-24.9673	0.0004%
Roll (rad)	-0.0149	-0.0153	2.6846%	0.0236	0.0238	0.8475%
Pitch (rad)	0.0009	0.0011	22.2222%	0.0025	0.0028	12.0000%
Yaw (rad)	0.0016	0.0015	-6.2500%	-0.0018	-0.0017	-5.5556%

6.3. Three-dimension dynamic response tracking under irregular waves

Meanwhile, the developed motion tracking method has been examined for floating structures under the consideration of irregular waves. In the experiment, the Jonswap spectrum has been used to simulate irregular waves with a period of 2s and a wave height of 0.12m. The Euler angle and acceleration of the structure measured by the gyroscope and accelerometer have been shown in Fig. 20. The response between 100s and 200s has been selected for data analysis. Finally, Fig. 21 and Table 3 have shown the results by the 6-DOF motion tracking system and the optical tracking device. It has been concluded that results of the proposed tracking system have maintained a good consistency with the measured data by the optical tracking device and proved the feasibility of the developed 6-DOF motion tracking system for tracking the marine floating structures in service.

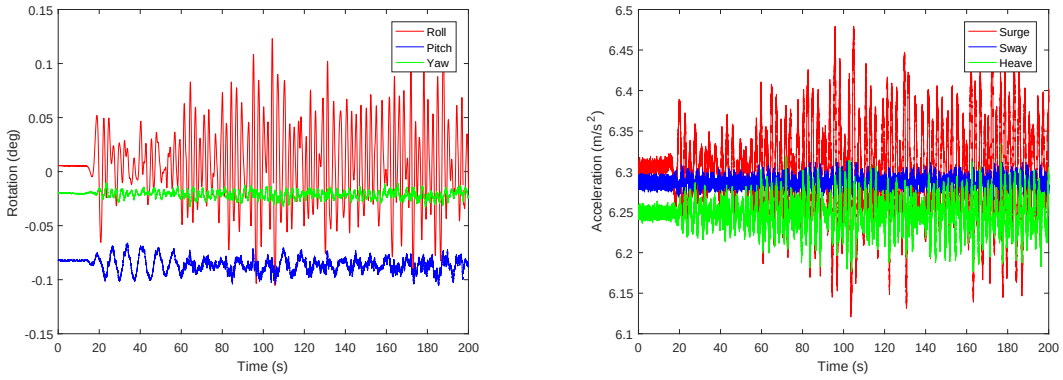

(a) (b)

Fig. 20: The (a) estimated Euler angle and (b) measured acceleration of the platform under irregular waves.

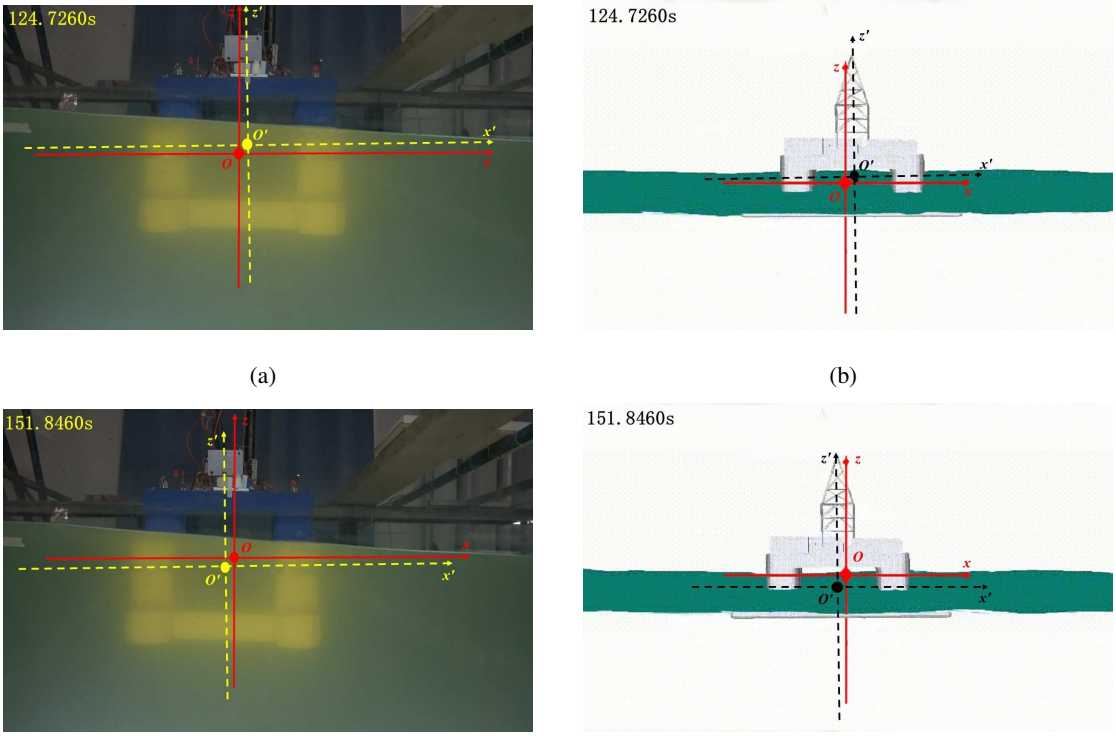

(a) (b)

(c) (d)

Fig. 21: The comparison results of the platform under regular waves between (Left) camera and (Right) the proposed method: (a) and (b) t=124.7260s; (c) and (d) t=151.8460s.

Table 3: 6-DOF motion tracking values of the platform under irregular waves.

Time	124.7260s			151.8460s		
	Measured results	Estimated results	Error	Measured results	Estimated results	Error
Surge (mm)	99.7803	99.7692	0.0111%	-77.2091	-78.0103	1.0377%
Sway (mm)	1.3652	1.3655	0.0220%	-0.5527	-0.5523	0.0724%
Heave (mm)	52.4229	52.4229	0.0000%	-23.4660	-23.4662	0.0009%
Roll (rad)	0.0994	0.0990	0.4024%	-0.0897	-0.0891	0.6689%
Pitch (rad)	-0.0210	-0.0213	1.4286%	-0.0205	-0.0200	2.4390%
Yaw (rad)	0.0524	0.0521	0.5725%	-0.0415	-0.0411	0.9639%

7. Summary and conclusions

This paper has proposed a 6-DOF motion tracking approach based on accelerations and angular velocities to accurately position the floating structures. In this method, the integral process of measured accelerations has been replaced by the calculation of complex exponential parameters to avoid the drift problem, and thus the 6-DOF motion tracking system of floating structures has been realized by the reconstruction of the relationship between accelerations and displacements. As compared with the optical non-contact measurement system, the proposed approach has demonstrated the excellent performance and higher measurement accuracy, owing to the effective prevention from environmental interference and data loss. The analysis results of an SDOF system show that the proposed displacement reconstruction method can be applied to the dynamic displacement reconstruction of floating structures. And simulation results of a semi-submersible platform by the Orcaflex under the considerations of the testing environment and equipment have shown that the maximum reconstruction error between the proposed approach and Orcaflex is around 1%, indicating the correctness of the developed tracking method.

To further verify the feasibility of the proposed approach applicable to complex marine structures, the semi-submersible platform has been carried out on a 1:100 model in a wave tank. It has been noted that the maximum absolute error between the proposed approach and the measured displacement by the optical device is only in the millimeter range. Considering the action of irregular waves, the maximum reconstruct error of 1% has been observed and the discrepancy of the displacement in the heave direction has been minimized by less than 0.5%. The meaningful results have demonstrated the superiority of the proposed approach over the optical devices for the motion tracking of floating structures and the great potential for a wider range of applications such as the heave response estimation in ocean engineering.

8. Acknowledgements

The authors acknowledge the financial support by the National Natural Science Foundation-Basic Science Center Project (52088102), the National Science Found for Distinguished Young Scholars of China (52125106) and the National Natural Science Foundation of China (U1806229).

References

Wu MN, Gao Z. Methodology for developing a response-based correction factor (alpha-factor) for allowable sea state assessment of marine operations considering weather forecast uncertainty. Mar Struct

2021;79:103050.

Zhang JH, Lu HC, Sun K. Dynamic response analysis for offshore structures by a combination of segmented responses based on pole-residue method. Ocean Eng 2021;219:108277.

Fu SX, Moan T. Dynamic analyses of floating fish cage collars in waves. Mar Struct 2012;47:7-15.

Wei W, Fu SX, Moan T, Song CH, Ren TX. A time-domain method for hydroelasticity of very large floating structures in inhomogeneous sea conditions. Mar Struct 2018;57:180-192.

Ai CF, Ma YX, Yuan CF, Dong GH. Non-hydrostatic model for internal wave generations and propagations using immersed boundary method. Ocean Eng 2021;225:108801.

Veltcheva A, Soares CG. Nonlinearity of abnormal waves by the HilbertCHuang Transform method. Ocean Eng 2016;115:30-38.

Liu FS, Gao SJ, Tian Z, et al. A new time-frequency analysis method based on single mode function decomposition for offshore wind turbines. Mar Struct 2020;72:102782.

Kim S, Park K-Y, Kim H-K, Lee HS. Damping estimates from reconstructed displacement for low-frequency dominant structures. Mech Syst Signal Pr 2020;136:106533.

Wu WH, Wang YL, Tang D, et al. Design, implementation and analysis of full coupled monitoring system of FPSO with soft yoke mooring system. Ocean Eng 2016;113:255-263.

Prislin I, Halkyard J, Debord F, et al. Full-scale measurement of the Oryx Neptune production spar platform performance. Proceedings of the Offshore Technology Conference, Houston, 1999.

Edwards R, Prislin I, Johnson T, et al. Review of 17 real-time, environment, response, and integrity monitoring systems on floating procuction platforms in the deep waters of the Gulf of Mexico. Proceedings of the Offshore Technology Conference, Houston, 2005.

Du Y, Wu WH, Yue QJ. Prototype measurement for deep water floating platforms based on monitoring technology. Proceedings of the 32nd International Conference on Ocean, Offshore and Artic Engieering, Nantes, 2013.

Mitikiri YB, Mohseni K. A geometric framework for rigid body attitude estimation. Automatica 2021;128:109494.

Chen XQ, Cao L, Guo PY, Xiao B. A higher-order robust correlation Kalman filter for satellite attitude estimation. ISA T 2019; Available online.

Chen PY, Guan T, Zhang GB, et al. Three dimensional stabilization controller based on improved quaternion transformation for fixed-wing UAVs. ISA T 2021; Available online.

Nezhadshahbodaghi M, Mosavi MR. A loosely-coupled EMD-denoised stereo VO/INS/GPS integration system in GNSS-denied environments. Measurements 2021;183:109895.

Chen HB, Moan T, Verhoeven H. Effect of DGPS failures on dynamic positioning of mobile drilling units in the North Sea. Accident Anal Prev 2009;41(6):1164-1171.

Liagre P, Gupta H, Banon H. Monitoring of floating offshore installations' wave frequency motions. Proceedings of the Offshore Technology Conference, Houston, 2008.

Teigen P, Haver S. The Heidrun TLP: measured versus predicted response. Appl Ocean Res 1998;20(1):27-35.

Damaris A-L, Jaime DI-C Assessment of methodologies to estimate displacements from measured acceleration records. Measurement 2018;114:261-273.

Hong YH, Kim H-K, Lee HS. Reconstruction of dynamic displacement and velocity from measured accelerations using the variational statement of an inverse problem. J Sound Vib 2010;329(23):4980-5003.

Gao SJ, Liu FS, Jiang CY. Improvement study of modal analysis for offshore structures based on reconstructed displacements. Appl Ocean Res 2021;110:102596.

Zheng WH, Dan DH, Cheng W, Xia Y. Real-time dynamic displacement monitoring with double integration of acceleration based on recursive least squares method. Measurement 2019;141:460-471.

Liu FS, Gao SJ, Chang S. Displacement estimation from measured acceleration for fixed offshore structures. Appl Ocean Res 2021;113:102741.

Makdah AARA, Daher N, Asmar D, Shammas E. Three-dimensional trajectory tracking of a hybrid autonomous underwater vehicle in the presence of underwater current. Ocean Eng 2019;185:115-132.

Grigoryan AM, Agaian SS. Commutative quaternion algebra and DSP fundamental properties: Quaternion convolution and Fourier transform. Signal Process 2022;196:108533.

Urynbassarova D, Teali AA, Zhang F. Discrete quaternion linear canonical transform. Digit Signal Process 2022;122:103361.

Li YM, Li Y, Wu Q. Design for three-dimensional stabilization control of underactuated autonomous underwater vehicles. Ocean Eng 2018;150:327-336.

Weng YS, Wang SD, Zhang HC, et al. A high resolution tilt measurement system based on multi-accelerometers. Measurement 2017;109:215-222.

Hu S-LJ, Yang WL, Li HJ. Signal decomposition and reconstruction using complex exponential models. Mech Syst Signal Pr 2013;40(2):421-438.

Golub GH, Loan CFV, Matrix Computations, 3rd edition. Johns Hopkins University Press, Baltimore, MD, 1996.

Liu FS, Gao SJ, Liu DZ, Zhou H. A signal decomposition method based on repeated extraction of maximum energy component for offshore structures. Mar Struct 2020;72:102779.

Gao SJ, Liu FS, Chang S, Zhou L. A dynamic response analysis method with high-order accuracy for fixed offshore structures based on a normalised expression of external loadings, Ocean Eng 2021;219:108358.

Cummins WE. The impulse response function and ship motions, Schiffstechnik 1962;9:101-109.

Liu FS, Chen JF, Qin HD. Frequency response estimation of floating structures by representation of retardation functions with complex exponentials, Mar Struct 2017;54:144-166.

Lu HC, Tian Z, Zhou L, Liu FS. An improved time-domain response estimation method for floating structures based on rapid solution of a state-space model, Ocean Eng 2019;173:628-642.

Giovanni A A, Celso P P, Guilherme R F. Mooring system stiffness: A six-degree-of-freedom closed-form analytical formulation, Mar Struct 2022;84:103189.

Yu LW, Li CL, Wang SQ. Model tests and numerical simulations on the parametric resonance of the deep draft semi-submersible under regular waves, Ocean Eng 2022;243:110273.